Journal of Power Sources 182 (2008) 630–638

Contents lists available at ScienceDirect

Journal of Power Sources

journal homepage: www.elsevier.com/locate/jpowsour

Active (air-cooled) vs. passive (phase change material) thermal management of high power lithium-ion packs: Limitation of temperature rise and uniformity of temperature distribution

Rami Sabbah, R. Kizilel, J.R. Selman, S. Al-Hallaj*

Center for Electrochemical Science and Engineering, Department of Chemical and Biological Engineering, Illinois Institute of Technology, 10 W. 33rd Street, Chicago, IL 60616, USA

ARTICLE INFO

Article history:
Received 21 January 2008
Received in revised form 21 March 2008
Accepted 21 March 2008
Available online 8 April 2008

Keywords:
Phase change material
Li-ion batteries
Thermal management
Active cooling
Passive cooling
High discharge rates

ABSTRACT

The effectiveness of passive cooling by phase change materials (PCM) is compared with that of active (forced air) cooling. Numerical simulations were performed at different discharge rates, operating temperatures and ambient temperatures of a compact Li-ion battery pack suitable for plug-in hybrid electric vehicle (PHEV) propulsion. The results were also compared with experimental results. The PCM cooling mode uses a micro-composite graphite–PCM matrix surrounding the array of cells, while the active cooling mode uses air blown through the gaps between the cells in the same array. The results show that at stressful conditions, i.e. at high discharge rates and at high operating or ambient temperatures (for example 40–45 °C), air-cooling is not a proper thermal management system to keep the temperature of the cell in the desirable operating range without expending significant fan power. On the other hand, the passive cooling system is able to meet the operating range requirements under these same stressful conditions without the need for additional fan power.

1. Introduction

Management of heat effects associated with lithium-ion batteries remains a challenge as excessive local temperature rise in Li-ion cells causes reduction of cycle life and may lead to thermal runaway of individual cells or of an entire battery pack [1]. Especially in battery packs where the cells are closely packed, in order to exploit the advantage of Li-ion's high energy and power density, thermal runaway of a cell can propagate and cause an entire battery to fail violently [2]. More frequently, excessive or uneven temperature rise in a module or pack reduces its cycle life significantly. However, for commercial application it is important not to overdesign the cooling system and unnecessarily complicate the control hardware. Hence, interest is emerging in passive thermal management, that is, a cooling system which requires no blowers and flow distributors, or at most very simplified ones, to maintain the temperature and thermal profile within the desired range. This paper analyzes the cooling performance of a form of passive thermal management which makes use of phase change material (PCM). Companion papers of this study show that a PCM-based cooling system can preserve the compactness and light-weight advantages of Li-ion compared to NiMH technology [3], and that it can prevent serial thermal runaway in Li-ion battery packs [4].

Khateeb et al. [5] first demonstrated successfully a passive thermal management system, patented by Al-Hallaj and Selman [6,7], is capable of replacing conventional thermal management system for Li-ion batteries in EV and electric scooter applications. In this passive system, a PCM-containing matrix, for example certain mixtures of waxes or wax-like materials form a micro-composite with a thermally conducting material such as graphite [3,8,9]. This greatly improves the rate of heat removal from the PCM-composite to the ambient atmosphere (or to the cell) by conduction, while keeping the high thermal capacity due to the latent heat of phase change almost unchanged.

Initial analysis and experiments on high energy Li-ion cells [8,9] have shown that even under stressful operating conditions the matrix of PCM/graphite composite keeps the temperatures of individual cells in a favorable range, similar to that achieved by air-cooling, with very good temperature uniformity from cell to cell. Because of its simplicity and dual function as buffer and conductor, such a PCM-based passive cooling device may become an important component of the thermal management of advanced Li-ion batteries.

* Corresponding author. Tel.: +1 312 567 5118; fax: +1 312 567 6914.
E-mail address: alhallaj@iit.edu (S. Al-Hallaj).

0378-7753/$ – see front matter © 2008 Elsevier B.V. All rights reserved.
doi:10.1016/j.jpowsour.2008.03.082

Nomenclature

A	cross-sectional area (m^2)
C	solid specific heat capacity ($J\,(kg\,K)^{-1}$)
C_p	gas specific heat capacity ($J\,(kg\,K)^{-1}$)
E	internal energy ($J\,m^{-3}$)
h	enthalpy ($J\,m^{-3}$)
hc	heat transfer coefficient ($W\,(m^2\,K)^{-1}$)
h_d	hydraulic diameter (m)
I	identity matrix
k	thermal conductivity ($W\,(m\,K)^{-1}$)
$\dot{m}$	air mass flow rate ($kg\,s^{-1}$)
M	mass (kg)
p	pressure (Pa)
q	heat generation rate ($W\,m^{-3}$)
R	gas constant ($m^2\,(s^2\,K)^{-1}$)
Re	Reynolds number, $Re = \rho v h_d/\mu$ (dimensionless)
t	time (s)
T	temperature (K)
$\vec{v}$	velocity vector ($m\,s^{-1}$)
$\dot{V}$	air volumetric flow rate ($m^3\,s^{-1}$)

Greek symbols

β	liquid fraction
η	performance index (dimensionless)
θ	normalized cell temperature (dimensionless)
λ	PCM latent heat ($J\,kg^{-1}$)
μ	dynamic viscosity $(kg\,(m\,s)^{-1}$
ρ	density ($kg\,m^{-3}$)
τ	stress tensor (Pa)

Subscripts

a	area averaged
c	cell
ca	cell surface area averaged
f	fluid (air)
in	inlet
l	liquid phase
m	mean (average)
out	outlet
pcm	phase change material
s	solid phase
v	volume averaged
w	wall
3 A	3 A discharge rate
10 A	10 A discharge rate

Superscripts

-	averaged
max	maximum
min	minimum

2. Objective and methodology

In this study, we compare the active vs. passive thermal management systems during normal and stressful discharge protocols. To help visualize the results, we focus on a high power Li-ion battery pack suitable for PHEV applications. Various flow rates of air at different cooling rates are tested in order to determine the pros and cons of each mode of cooling. The effectiveness of the cooling mode (active vs. passive) is determined by the relative capability to lower the cell temperature, and to keep temperature uniformity along the pack (in the active-cooling flow direction). This comparison is carried out for various levels of discharge rate, and for various initial and ambient temperatures.

In the case of active cooling (forced air flow), the fan power required not to exceed a certain value and the cell temperature or non-uniformity of thermal profile may serve as a figure of merit. On the other hand, in the case of passive (PCM) cooling, the effectiveness of the PCM component depends on the ratio of the PCM to the total pack volume, as well as the ambient temperature.

It is important to keep in mind that the passive thermal management of the pack studied in this work is only approximately optimized. The volume and mass ratios of PCM matrix to cell in the battery pack, as well as the exact composition of the PCM–graphite composite may be further optimized. The main purpose here is a proof of principle of passive (PCM) cooling under stressful operating and ambient conditions, in comparison to traditional active cooling. The conditions chosen target the theoretical replacement of the NiMH battery pack of a Hybrid Ford Escape with a lithium-ion battery pack from state-of-the-art high power Type 18650 Li-ion cells.

3. Mathematical model

A pack consists of 68 modules with 4S5P design (4 cells in series and 5 strings in parallel) is selected for this study. The pack is similar to an actual Li-ion battery pack which has been tested by our research group in a project co-sponsored by the City of Chicago and in collaboration with National Renewable Research Energy Laboratory and other industrial partners (Fig. 1a). The pack was specifically designed for a Ford Escape Hybrid in order to replace the existing NiMH battery pack and each module contains 20 commercially available 1.5 Ah Type 18650 high power Li-ion cells. The nominal voltage and capacity of each module is 14.4 V and 7.5 Ah, respectively. The whole pack is fitted in a plastic casing where air flows in the Z-direction as shown in Fig. 1b.

The design of the air-cooling system ensures the uniformity of the air flow between the cells (the air volumetric rate between the cells in the pack is the same). The pack casing is assumed to be thermally insulated. Such condition makes it possible to use the symmetry for flow and heat in the pack where it is possible to model a 90° sector (Fig. 1b). Fig. 1b also shows four cells (in series) and the air gap in the X–Y plane. However, three-dimensional air flow is considered due to contraction at the entrance and expansion at the exit of the battery module (Fig. 2). An 3D flow model will clearly show the temperature variation in all directions. Fig. 2 also depicts the domain used for air-cooling which consists of 90° sector of the four cells in series, the air upstream the cell, air downstream the cell, and the air in the gap between the cells.

Contrary to air-cooling, interstitial gaps in the pack are filled with graphite/PCM-composite material in passive cooling; the pack is insulated from all sides which ratify 2D approach. The temperature variation along the Z-direction becomes negligible. Fig. 1b shows the domain occupied by the cell and the domain occupied by the graphite/PCM material. Specifications of Li-ion cells and the interstitial spaces used in the modeling are summarized in Table 1.

Table 1
Modeling parameters for 18,650 Li-ion cells

	Diameter (mm)	Length (mm)	Hydraulic diameter (mm)	Cross-sectional area (mm^2)
Cell	18.2	65	18.2	260
Inter-cell gap	NA	65	5	71

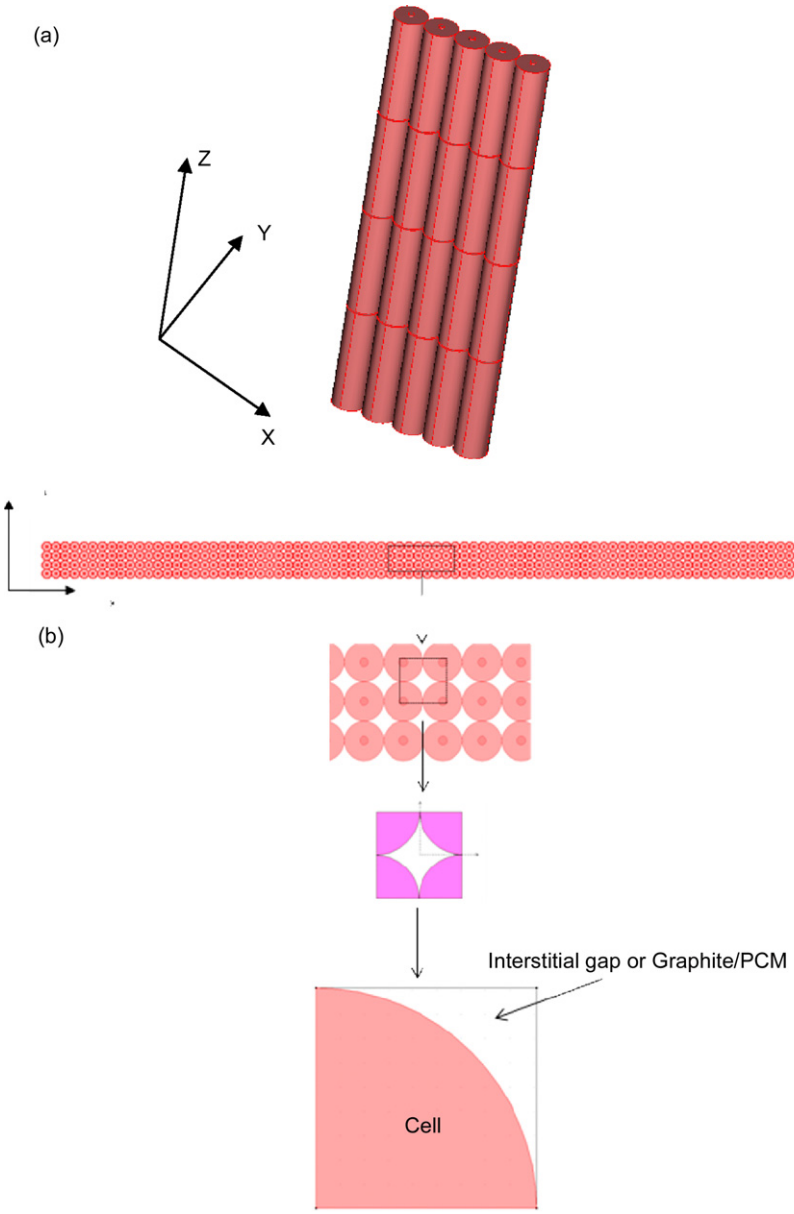

Fig. 1. (a) Lithium-ion battery 4S5P module 3D schematic. (b) Schematics of 2D of the pack and the selected domain for modeling.

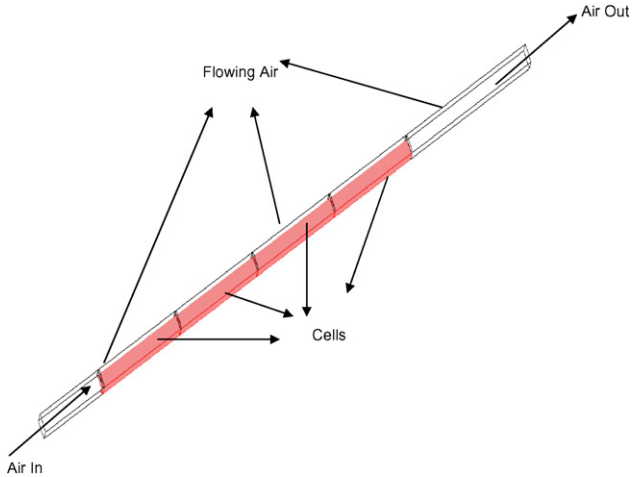

Fig. 2. Schematics of 3D air-cooling model.

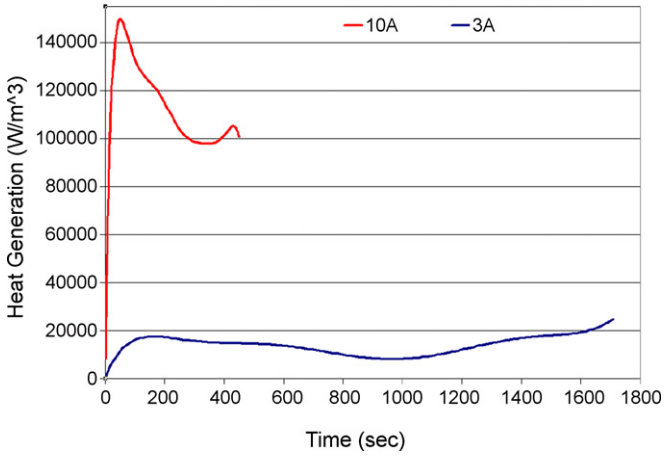

Fig. 3. Volumetric heat generation rates for 3 A and 10 A discharge rates measured by ARC.

The thermal profiles and fluxes are modeled by a single and complete discharge at a given constant current (*C* rate). These profiles and fluxes therefore are transient. However, the ambient conditions (temperature and, in the case of active cooling, entrance flow rate and temperature) are assumed constant.

3.1. Modeling of active cooling system (air-cooling)

In this part of the work, a transient 3D model is used to simulate the heat transfer within the pack. Heat is generated at any point in the high power Li-ion cell and determined experimentally by Accelerating Rate Calorimetry (ARC). The pack maintains the constant volumetric flow rate of air and involves a contraction when the air enters the interstitial spaces and an expansion when the air exits. This type of behavior results in a significant pressure drop along the pack and requires fan power in order to keep the volumetric flow rate constant. Moreover, contraction and expansion results in significant cooling at the two ends of each module. Therefore, 5 cm upstream flow and 10 cm downstream are taken into account to establish the effect of contraction and expansion in order to determine any pressure drop and therefore fan power on applied load and ambient condition. The thermal and hydraulic properties of air are considered as temperature dependent. The air is considered as ideal gas, and viscous dissipation is neglected.

3.1.1. Governing equations

Standard conservation equations of continuity, momentum and energy equations are used for the flowing fluid (air) domain, whereas only an energy balance was used for the cell domain.

The continuity equation and momentum balance are given by Eqs. (1) and (2), respectively. The nomenclature for each parameter can be found at the beginning of the paper.

$$\frac{\partial \rho_f}{\partial t} + \nabla(\rho_f \vec{v}_f) = 0 \tag{1}$$

$$\frac{\partial(\rho_f \vec{v}_f)}{\partial t} + \nabla(\rho_f \vec{v}_f \vec{v}_f) = -\nabla p_f + \nabla(\bar{\tau}_f) \tag{2}$$

The stress tensor is defined according to Eq. (3):

$$\bar{\tau}_f = \mu_f \left[(\nabla \vec{v}_f + \nabla \vec{v}_f^T) - \frac{2}{3} \nabla \vec{v}_f I \right] \tag{3}$$

The energy equation for air is given by Eq. (4):

$$\frac{\partial(\rho_f E_f)}{\partial t} + \nabla(\vec{v}_f(\rho_f E_f + p_f)) = \nabla(k_f \nabla T_f) \tag{4}$$

Here the internal energy is related to enthalpy and temperature in the usual way by Eq. (5), assuming ideal gas behavior as represented in Eqs. (6) and (7):

$$E_f = h_f - \frac{p_f}{\rho_f} + \frac{v_f^2}{2} \tag{5}$$

$$\rho_f = \frac{p_f}{R_f T_f} \tag{6}$$

$$h_f = \int_{T_{ref}}^{T_f} C_{pf}\, dT_f \tag{7}$$

The energy equation for the cell domain takes the simplified form of Eq. (8):

$$\frac{\partial(\rho_c C_c T_c)}{\partial t} = \nabla(k_c \nabla T_c) + q \tag{8}$$

Experimentally determined heat generation term q are shown in Fig. 3, and are fitted into polynomial equations by using least square methods.

The heat transfer coefficient between air and the cells is calculated according to Eq. (9):

$$\mathrm{hc} = \frac{q_w}{T_w - T_m} \tag{9}$$

and the mean flow temperature (T_m) is calculated according to Eq. (10):

$$T_m = \frac{\int \rho_f \vec{v}_f T_f \, dA}{\int \rho_f \vec{v}_f \, dA} \tag{10}$$

3.1.2. Initial and boundary conditions

Fig. 1b depicts that two sides of the square are part of cell and benefit from the symmetry whereas the other two boundaries represents a quarter of the equally divided interstitial gap which also benefits from symmetry, in other words zero heat flux. Mass flow rate and the temperature of inlet air are both constant. On the other hand, a convective heat flux is assumed at the outlet of the air domain whereas the gage pressure is considered as zero gage pressure.

At the cell/air interface a no-slip boundary condition is applied, as well as continuity of heat flux between the cell and the flowing air.

It should also be noted that in this model the heat transfer between the cell and flowing ambient air is not explicitly related to temperature difference by a heat transfer coefficient hc. However, to facilitate interpretation of the results, the heat transfer coefficient between air and the cell is calculated according to Eq. (9) where q_w is the heat flux at the cell wall, and T_w is the cell wall temperature.

3.2. Passive cooling (graphite–PCM matrix)

To compare passive cooling with active cooling, the same geometry as in Fig. 1b was used with PCM-composite filling the inter-cell gaps. Earlier studies [8,9] have shown that PCM provides uniformity along the longitudinal cell dimension (*Z*-axis) in modules or packs, therefore, a 2D transient model rather that a 3D transient model was adopted. The contact resistance between cell and PCM-composite was assumed to be negligible, while the top and bottom cell surfaces were assumed to be thermally insulated

3.2.1. Governing equations

Only the energy conservation equation was used to model both cell domain and PCM domain. Eq. (8) is again valid for the energy balance equation of the cell, while the energy balance equation for PCM is defined by Eq. (11):

$$\frac{\partial(\rho_{pcm} C_{pcm} T_{pcm})}{\partial t} = \nabla(k_{pcm} \nabla T_{pcm}) \tag{11}$$

The specific heat of PCM/graphite ($C_{p_{pcm}}$) in Eq. (11) requires some modifications. It is an effective property designed to account for the latent heat upon melting. It is therefore highly dependent on the phase of the PCM material in the graphite/PCM-composite. Experimental studies show that a PCM material such as wax usually has a *melting range* rather than a melting point, as it is usually a mixture of paraffin-type hydrocarbons or their derivatives. The melting range therefore needs empirical determination [5]. The PCM material is entirely solid below the melting point, and entirely liquid above the liquefaction point. Therefore (C_{pcm}) is constant below the melting point and above the liquefaction point. Mills et al. showed that (C_{pcm}) depends on the fraction liquid, β, and the details can be found elsewhere [10].

3.2.2. Initial and boundary conditions

The initial and boundary conditions for the passive (PCM) cooling process are identical to those for the active cooling system. This

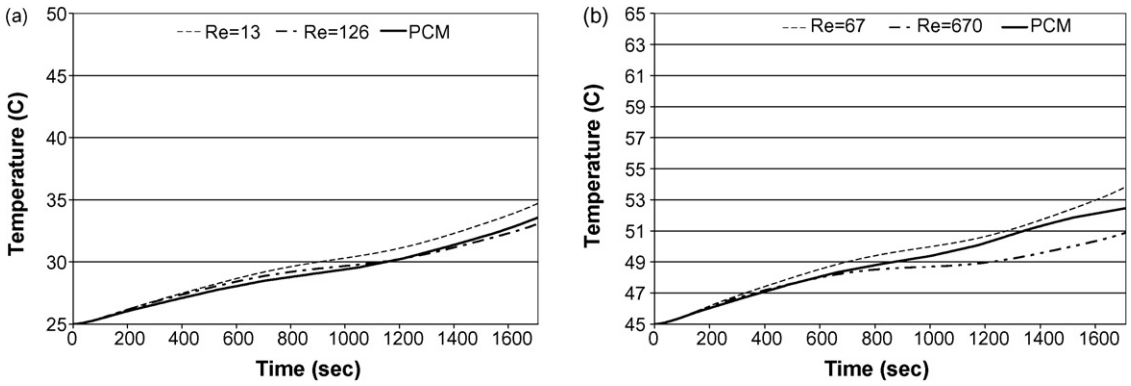

Fig. 4. Comparison of cooling systems based on volume averaged cell temperature at 3 A: (a) T_{amb} = 25 °C and (b) T_{amb} = 45 °C.

Table 2
Electrical characteristics of the Li-ion cell

Cell	18650
Capacity (Ah)	1.5
Maximum voltage (V)	4.2
Nominal voltage (V)	3.7
Minimal voltage (V)	3.0
Max discharge rate (A)	20 (13.33 *C*)

is due to the symmetry viewed from the four lateral surfaces. In addition to symmetry, temperature and heat flux are continuous at the PCM/cell interface.

4. Input data and physical properties

The commercially available cells used in this study were discharged from 100% SOC to 15% SOC in a single discharged. Discharge rates of 2 and 6.67 *C*-rates used in this study can be performed safely. The specifications for the Type 18650 high power commercial Li-ion cell are shown in Table 2. Thermo-physical properties of the Type 18650 high power cell, and the PCM-composite are shown in Table 3.

5. Model output

- The modeling calculations involve the following outputs: volume average cell temperature as a function of time and state-of-discharge:

$$\bar{T}_{cv} = \frac{\int T_c \, dV_c}{\int dV_c} \tag{12}$$

- Profile of maximum temperature difference along the pack at the state-of-discharge.
- Power required to maintain constant flow velocity during a discharge:

$$FP = \dot{V} \, \Delta P \tag{13}$$

- Comparison of modeling and experimental results in terms of surface temperature.

To facilitate interpretation of the results (below), secondary output parameters are used as follows:

In active (air flow) cooling:

- The mean flow temperature of the air (T_m), calculated according to Eq. (10).
- The heat transfer coefficient between cell and flowing air, as in Eq. (9), as well as the Reynolds number of the air flow in the air gap between four cells.

In passive (PCM) cooling:

- The area average liquid fraction of the PCM (β) at any time averaged over the PCM domain according to Eq. (14):

$$\bar{\beta} = \frac{\int \beta \, dA_{pcm}}{\int dA_{pcm}} \tag{14}$$

In both active cooling and passive cooling:

- The cell maximum temperature difference (CMTD), defined as the largest difference in the local cell temperature (T_c) between any points in the pack domain of the model:

$$dT_{max} = T_c^{min} - T_c^{min} \tag{15}$$

- The cooling index (η): which is the ratio of the heat dissipated from the cell into air to the energy required to power the cooling fans (Eq. (16)):

$$\eta = \frac{\int \dot{m} C_{pf} (T_{out} - T_{in}) dt}{\int \dot{V} \, \Delta P \, dt} \tag{16}$$

where $\dot{m}$ is the air mass flow rate, C_p is the air specific heat capacity, T_{out} is the air temperature at the outlet, T_{in} is the air temperature at the inlet, $\dot{V}$ is the air volumetric flow rate, and ΔP is the pressure drop between the inlet and the outlet.

Table 3
Thermo-physical properties of the Type 18650 high power cell, and the PCM-composite

	Density (kg m^{-3})	Specific heat (J (kg K)$^{-1}$	Thermal conductivity (W m^{-2} K)	Melting range (C)	Latent heat (J kg^{-1})
Cell	2663	900	Radial = 3 Axial = 30	NA	NA
PCM	866	1980	16.6	52–55	181,000

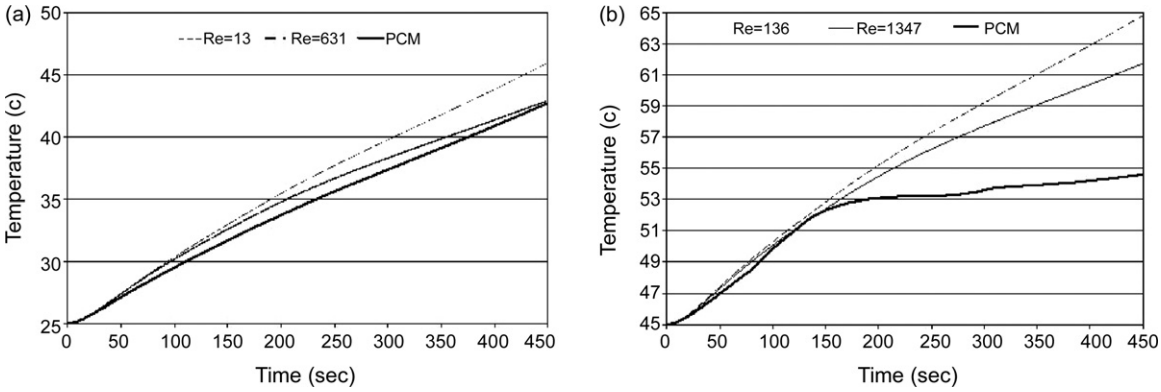

Fig. 5. Comparison of cooling systems based on volume averaged cell temperature at 10 A: (a) T_{amb} = 25 °C and (b) T_{amb} = 45 °C.

6. Results

The heat generation at 10 A and 3 A are determined and shown in Fig. 3. It is clearly seen from the figure that the heat generation for high current (10 A) is significantly higher than the one at low current (3 A). This is due to the higher ohmic resistance at high current. It is anticipated that an improper usage of a cooling system will result in significant increase in temperature at higher currents. On the other hand, the heat generation is relatively uniform and low at 3 A which makes it easier to control the temperature of the pack at a desired temperature range with a proper thermal management system.

The need for safe containment and management of appreciable heat effects associated with lithium-ion batteries in high power applications remains a challenge to be met before wide-spread commercialization can occur [5]. Therefore, to keep the temperature of the pack at low level is the main goal of this study. To achieve low temperature, various air flow rates were attempted to remove the generated heat from the cells. Temperature profiles of a cell in the pack during discharge at 25 °C and 3 A are shown in Fig. 4a. It is clearly seen that the temperature of a cell is kept below 35 °C at all cooling schemes. Superiority of air-cooling to PCM cooling or vice versa is not the case for this condition. Active and passive management systems are sufficient due to the low heat generation at 3 A. On the other hand, when the ambient temperature is 45 °C, air-cooling is still capable of keeping the local cell temperature at the 2C discharge below 55 °C, which was selected as the maximum allowable temperature in this study, but this requires a higher flow rate (Re = 67). Also when the operating temperature of the pack is raised from 25 °C to 45 °C, cooling at high Re shows lower cell temperature compared to passive cooling (Fig. 4b). However, Fig. 4b also depicts that lowering air velocity or Re for one order of magnitude results in higher final temperature for active cooling. Nevertheless, temperature of the cell may be kept below 55 °C in all cases and either of the thermal management system suits well.

Increase of current from 3 A to 10 A requires an efficient cooling as the heat generation increases significantly. Fig. 5a and b show the advantage of using PCM as it starts to utilize the latent heat of the paraffin wax. To keep cell temperature below 55 °C, one should increase the velocity of the air flow significantly (Re = 631). By increasing the velocity of the air for about 50 times, the temperature of the cell can be brought down for only 45.7–49.0 °C. A clear advantage of using PCM can be seen in Fig. 5b for the case of 45 °C ambient temperature and discharge current of 10 A. The temperature keeps increasing during active cooling no matter how high the laminar flow is exceeding 55 °C less than halfway during discharge. Ramadass et al. [11] reported significant increase in capacity fading for commercial 18,650 cells when operating temperature increased from 45 °C to 50 °C [11]. On the contrary, if PCM is used as thermal management system (Fig 5b), the temperature is always kept below 55 °C. Therefore, under moderate conditions of either current load or ambient temperature, or both, passive (PCM) cooling performs equally well as active cooling. Under "normal", that is non-stressed, conditions the two modes of cooling are comparable in effectiveness.

Table 4
Temperature rise at various operating conditions

I = 3 A T_{amb} = 25 °C		I = 3 A T_{amb} = 45 °C		I = 10 A T_{amb} = 25 °C	
Re	ΔT (°C)	Re	ΔT (°C)	Re	ΔT (°C)
13	0.58	67	1.62	13	0.8
126	1.84	670	2.06	631	4.2
PCM	0.03	PCM	0.14	PCM	0.07

The maximum temperature difference which the cells experience during a discharge is another important point from the viewpoint of cycle-life of the Li-ion battery pack. This is especially of importance since it is known that active cooling at high rates induce appreciable non-uniformity of temperature in a pack (Table 4).

A measure of this non-uniformity is the CMTD defined in Section 5. Table 4 summarizes the CMTD for various current loads and ambient temperatures. The results show that CMTD for passive cooling does not exceed 0.5 °C in the case of stressful conditions (6.67 C-rate and 45 °C ambient temperature), while for the normal conditions the CMTD in passive cooling is almost negligible.

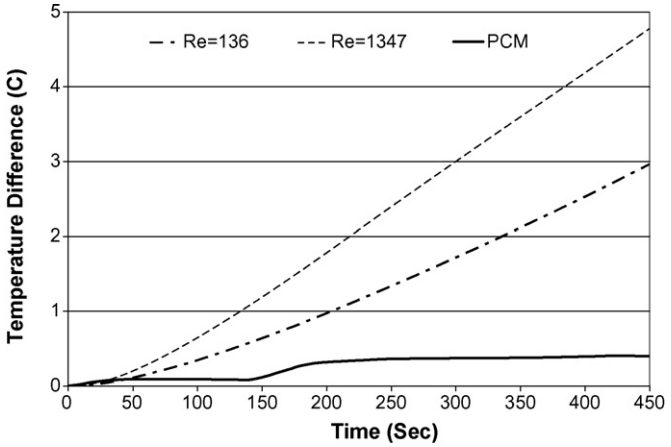

Fig. 6. Comparison of air-cooling (for Re = 136, ReR = 1347) vs. passive cooling using PCM on volume averaged cell temperature at 10 A discharge rate and 45 °C.

Table 5
Maximum temperature and fan power required at 3 A and various operating conditions

T_{amb} = 25 °C			T_{amb} = 45 °C		
Re	*T* (°C)	FP (W)	*Re*	*T* (°C)	FP (W)
13	34.72	0.0046	67	53.83	0.137
126	33.06	0.464	670	50.87	15.42
PCM	33.57	NA	PCM	52.45	NA

Table 6
Maximum temperature and fan power required at 10 A and various operating conditions

T_{amb} = 25 °C			T_{amb} = 45 °C		
Re	*T* (°C)	FP (W)	*Re*	*T* (°C)	FP (W)
13	45.95	0.0007	67	64.80	0.8407
631	42.90	0.0707	670	61.72	10.7324
PCM	42.70	NA	PCM	54.60	NA

In active cooling, however, the CMTD reaches 2 °C in the case of 2 *C*-rate and up to 4.8 °C for 6.67 *C*-rate, regardless of the ambient temperature. It is also clear that the CMTD increases significantly with increasing flow rate, which makes the use of air-cooling under high-rate discharge undesirable and may shorten battery cycle-life. Fig. 6 compares the active and passive cooling at 10 A and 45 °C. When air-cooling is used for thermal management system, there is a significant temperature difference along the cell. The temperature difference in the cell increases with increasing the velocity of the air was estimated at 3.0 °C and 4.8 °C for *Re* = 136 and *Re* = 1347, respectively. On the other hand, the temperature variation along the cell is less than 0.4 °C when PCM cooling is used. As indicated above, a lower temperature gradient will greatly increase the battery cycle-life.

6.1. Fan power requirement

Cooling by forced air flow requires parasitic power to overcome the flow resistance of the narrow gaps in a compact Li-ion battery. Table 5 shows the average cell temperature and corresponding fan power required for various Reynolds numbers. It is obvious that air cooling which requires high flow rates (*Re* > 1000) needs significant fan power. For example, when the cells are discharged at 6.67 *C* and 45 °C ambient temperature, active cooling requires high flow rates (5 m s^{-1}) or high *Re* in order to keep the final cell temperature within the safety limit. The fan power needed for this case is about 73 W. Even then, the mean cell temperature was 7 °C higher than the safety limit of 55 °C. Further decrease in maximum temperature in the cell would necessitate operating in the turbulent range and therefore appreciably increase the required fan power (Table 6).

Required fan power is also calculated in terms of cooling index in order to see the effect of flow rate on the fan power. Table 7 shows values for the cooling indexes at different operating conditions. Results show that the cooling index is high at low *Re* where only a small portion of the power is used to keep the temperature below 55 °C. However, as the flow rate or *Re* increases, the required power increases and becomes comparable to the heat dissipated in the pack and therefore cooling index decreases. In other words, when the flow rate is high (*Re* > 1000) the fan power is of the order of the energy dissipation in the cell. Therefore, the fan power requirement is not an essential argument against active cooling, and in favor of passive (PCM) cooling. More important though is the consequence of high flow rates for the non-uniformity of cell temperatures within the pack, and (especially if larger cells are used than the Type 18650 in this study) for thermal non-uniformity within the cell.

Table 7
Cooling indexes at various operating conditions

T_{amb} = 25 °C			T_{amb} = 45 °C		
Current (A)	*Re*	Index	Current (A)	*Re*	Index
3	13	2918	3	67	455
3	126	221	3	135	188
3	–	–	3	630	13
10	13	5944	10	136	838
10	126	515	10	643	38
10	631	43	10	1347	8

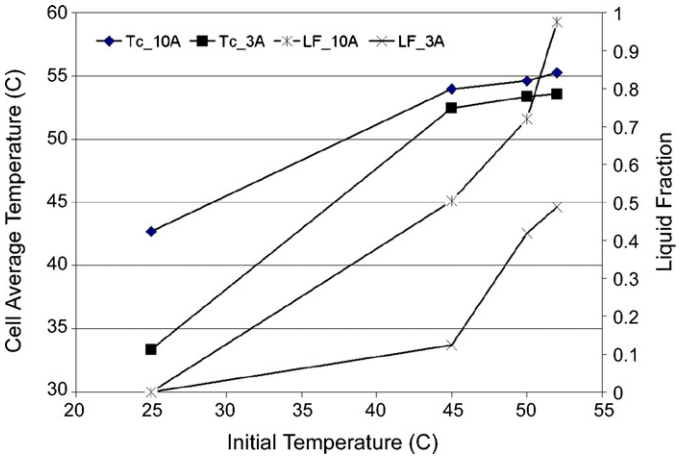

Fig. 7. Volume averaged cell temperature and volume averaged liquid fractions at the end of discharge for discharge rates 3 A and 10 A and 85%DOD.

6.2. Fraction of phase change in passive (PCM) cooling

Since passive cooling by PCM relies essentially on storage of the heat generated in a cell by phase change of the PCM (in addition to conduction of that heat by the PCM–graphite composite), the fraction liquid of the PCM is an important index of the progress of the cooling process and the effectiveness of the PCM itself.

Fig. 7 shows the final cell average temperature and the PCM liquid fraction after full discharge as a function of the ambient temperature, for both 2 (3 A) and 6.67 (10 A) rates. It is clear that passive (PCM) cooling keeps the cell temperature below 55 °C even when the ambient temperature is 52 °C during 6.67 *C*-rate. In this stressful case, most of the PCM melts. If the ambient temperature is lower, or the discharge rate is lower, little or none of the PCM melts. In that case the heat generated by the discharge of the cell is absorbed completely by the heat capacity of the cell and the solid PCM, while the temperature of the latter does not exceed 55 °C.

PCMs with different melting ranges may be used to accommodate different combinations of high ambient temperature and high discharge rate, while the solid phases (cell and PCM) have sufficient thermal conductivity and capacity to accommodate operating periods of lower ambient temperature or discharge rates. This is a distinct advantage of passive (PCM) cooling.

7. Model validation

7.1. Active air-cooling

An experimental set-up was built and tested in order to validate the mathematical model. Four Type 18650 high power cells in series were used in the test. The inner gab between the cells is the same as in the numerical model. The four cells were placed in a plexi-

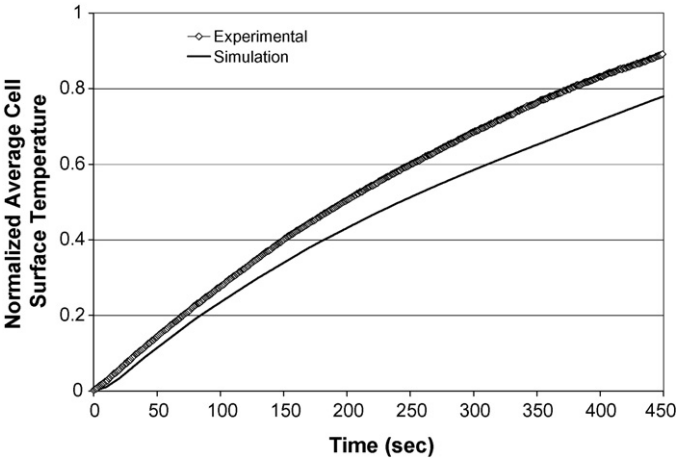

Fig. 8. Comparison of experimental and numerical normalized average cell surface temperature using air-cooling at 10 A, $Re = 405$, and $T_{amb} = 45\,^{\circ}C$.

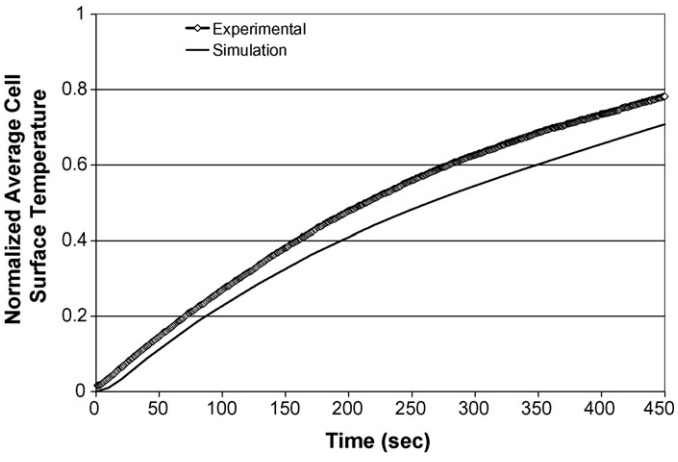

Fig. 9. Comparison of experimental and numerical normalized average cell surface temperature using air-cooling at 10 A, $Re = 882$, and $T_{amb} = 45\,^{\circ}C$.

glass duct which was thermally insulated. A powerful fan was used to generate the air flow and fine meshes were used for uniform air distribution. The orientation of the four cells is similar to the orientation of the cells in Fig. 1b. The fan speed was controlled by a TRIAC, a speed variator. The air flow rate (air speed) was measured by a digital Anemometer (Omega, Stamford, CT). Each cell was discharged at a constant current of 10 A using a battery cycler (Arbin, College Station, TX). The test apparatus was placed in a controlled environmental chamber. The chamber temperature was set to 45 °C. After the cells reached equilibrium temperature of 45 °C, the test was initiated. This procedure of testing insures that the initial cells temperature and air inlet temperature is 45 °C. Six T type thermocouples were attached to the cells in different locations in order to get an average temperature of the cells vs. discharge time. Two T type thermocouples were used to measure air inlet and outlet temperatures. Three tests were done for air-cooling, $Re = 406$, $Re = 882$, and $Re = 1353$. The initial and air inlet temperature was set to 45 °C. The results of these tests were compared with numerical results of the tested model under the same conditions. The results are presented in terms of the cell average surface temperature according to Eq. (17), because it was not possible to insert thermocouples inside the cells.

$$\bar{T}_{ca} = \frac{\int T\,dA_s}{\int dA_s} \tag{17}$$

The numerical model, presented in this work, was used to simulate the experimental set-up and compared to the experimental data. It should be noted here that the results presented before were presented in terms of the cells volume average temperature according to Eq. (16). That is, because the simulation results show the temperature everywhere in the cell, while in the experiment, it is only possible to measure the cell surface temperature.

Air inlet temperature fluctuated between 45 °C and 47 °C during the tests, therefore, the experimental and corresponding numerical results were normalized according to Eq. (18):

$$\theta = \frac{\bar{T}_{ca} - T_{in}}{\int q_{10A} dt / M_c C_c} \tag{18}$$

where T_{in} is air inlet temperature, $\bar{T}_{ca}$ is the surface area averaged cell temperature, q_{10A} is the heat generation rate for discharge rate of 10 A and given by Eq. (10), M_c is the cell mass, and C_c is the cell specific heat. The denominator in Eq. (18) represents the increase in cell temperature while thermally insulated.

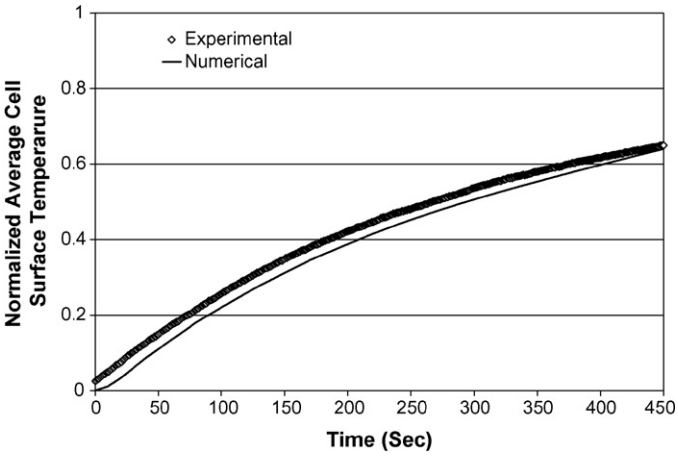

Fig. 10. Comparison of experimental and numerical normalized average cell surface temperature using air-cooling at 10 A, $Re = 1353$, and $T_{amb} = 45\,^{\circ}C$.

Figs. 8–10 show the normalized cell average surface temperature vs. time of discharge for discharge rate of 10 A, room temperature of 45 °C and for three air flow rates that correspond to $Re = 406$, 882, and 1353. The three figures show good agreement between numerical and experimental results. Both numerical and experi-

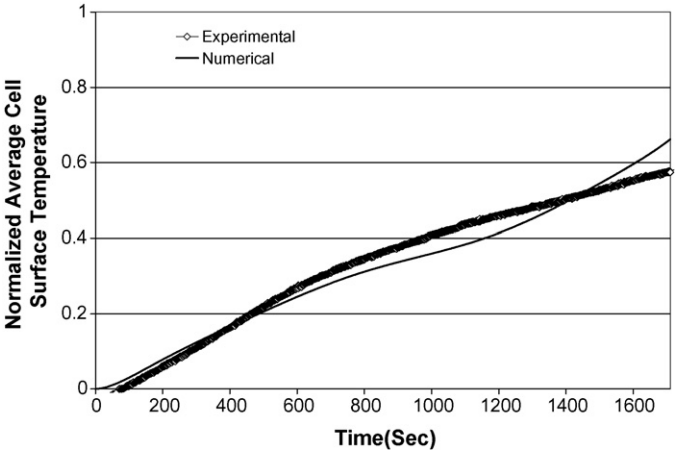

Fig. 11. Comparison of experimental and numerical normalized average cell surface temperature using PCM cooling at 3 A and $T_{amb} = 45\,^{\circ}C$.

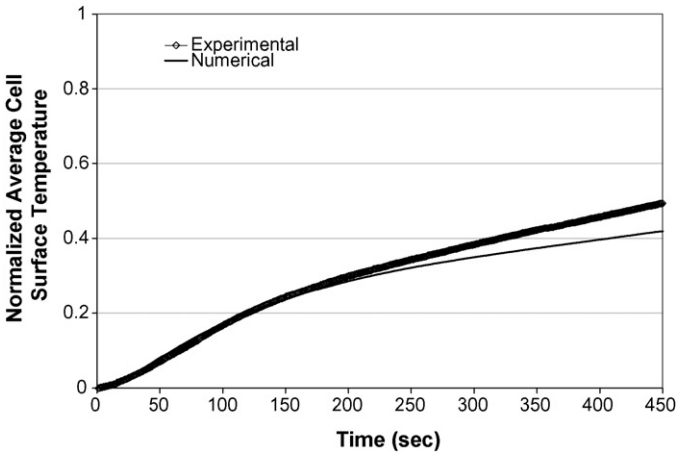

Fig. 12. Comparison of experimental and numerical normalized average cell surface temperature using PCM cooling at 10 A and T_{amb} = 45 °C.

mental results showed the same trend of increase in normalized cell average surface temperature vs. time. While higher Reynolds numbers showed better quantitative agreement than lower ones.

7.2. Passive cooling

A small pack with four cells on series was built in a PCM/graphite matrix with 3 mm spacing between the cells and 1.5 mm spacing on the edges. The selection of such dimensions was to ensure the symmetry in the pack. The pack was placed in the controlled temperature chamber and discharged using the battery cycler. Two tests were done for the above pack, 10 A discharge rate at 45 °C, and 3 A discharge rate at 45 °C. The cell temperature was averaged on the cell surface for the same reason mentioned in the previous section according to Eq. (17). Also, the surface area averaged cell temperature was normalized using Eq. (18) for the same reason mentioned earlier. Figs. 11 and 12 show the normalized surface area averaged cell temperature vs. discharge time, for two discharge rates of 3 A and 10 A, respectively. The results showed fairly good quantitative and qualitative agreement between numerical and experimental results.

8. Conclusion

Thermal modeling of a compact Li-ion battery pack suitable for PHEV application shows that passive cooling by PCM can keep the cell temperature in the pack below the upper safety limit (55 °C) in constant-rate discharge at rates as high as 6.67 *C* (10 A/cell) and under ambient temperatures as high as 45 °C, or even up to 52 °C. Under such stressed conditions, active cooling, which is adequate for moderate conditions of discharge rate and ambient temperature, cannot keep the cell temperature below the safety limit. Adequate active cooling at high discharge rates and high ambient temperature requires air flow rates close to or within the turbulent range which is not practical for vehicular applications.

While the expense of parasitic fan power under such conditions remains relatively small, the effect on non-uniformity of the cell temperatures within the pack is more appreciable (up to 5 °C for the above severe condition) and likely to impact battery cycle life. Passive (PCM) cooling, however, does not require fan power while keeping cell temperatures in the pack uniform.

The modeling results reported in this paper pertain to a suitably compact, but not optimized, pack configuration and to a standard, but not optimized composition of the PCM–graphite composite. Further optimization toward a targeted performance in EV or PHEV application is possible by utilizing the phase-change parameter (β) which is a by-product of the modeling reported here.

The numerical model is validated by a series of experiments done for both active cooling using air and passive cooing using PCM. Active cooling numerical results showed very good qualitative and good quantitative agreement with the experimental results, while passive cooling showed fairly good quantitative and qualitative agreement with the experimental results.

Acknowledgements

The authors are grateful for the financial and technical support provided by All Cell Technologies, LLC (Chicago, IL). The authors acknowledge Mohammed Khader, Abdul Lateef, and Peter Sveum for their technical support.

References

[1] E.P. Roth, Energy Conversion Engineering Conference and Exhibit 2000. 35th Intersociety, vol. 2, 2000, pp. 962–967.
[2] R.M. Spotnitz, J. Weaver, G. Yeduvaka, D.H. Doughty, E.P. Roth, J. Power Sources 163 (2007) 1080–1086.
[3] http://www.eere.energy.gov/vehiclesandfuels/pdfs/program/fc_fuel_partnership_plan.pdf, last accessed: March 18, 2008.
[4] J.R. Selman, R. Kizilel, R. Sabbah, S. Al-Hallaj, R. Spotnitz, A. Pesaran, G.H. Kim, The 7th International Advanced Automotive Battery and Ultracapacitor Conference (AABC-07), Long Beach, CA, May 14–18, 2007.
[5] S.A. Khateeb, M.M. Farid, J.R. Selman, S. Al-Hallaj, J. Power Sources 128 (2004) 292–307.
[6] S. Al-Hallaj, J.R. Selman, Novel Thermal Management of Battery Systems, US Patent 6,468,689 B1, October 22, 2002.
[7] S. Al-Hallaj, J.R. Selman, Battery System Thermal Management, US Patent 6,942,944 B2, September 13, 2005.
[8] S. Al-Hallaj, R. Kizilel, A. Lateef, R. Sabbah, M.M. Farid, J.R. S Selman, Proceedings of the 2005 IEEE Vehicle Power and Propulsion Conference VPPC, VPPC, 2005, pp. 376–380.
[9] R. Selman, R. Kizilel, R. Sabbah, S. Al-Hallaj, Proceedings of the 211th ECS Meeting, Chicago, IL, May 6–10, 2007.
[10] A. Mills, M.M. Farid, J.R. Selman, S. Al-Hallaj, Thermal conductivity enhancement of phase change materials using a graphite matrix, J. App. Therm. Eng. 26 (2006) 1652–1661.
[11] P. Ramadass, B. Haran, R. White, B.N. Popov, J. Power Sources 112 (2002) 606–613.